Mapping Karst Rock in Southwest China

Authors: Huang, Qiuhao, and Cai, Yunlong

Mapping Karst Rock in Southwest China

Qiuhao Huang[1] and Yunlong Cai[2]*

* Corresponding author: caiyl@urban.pku.edu.cn

[1] School of Geographic and Oceangraphic Sciences, Nanjing University, Hankou Road 22, Nanjing, Jiangsu Province 210093, People's Republic of China
[2] Department of Resources, Environment and Geography, Center for Land Study, Room 3355, YiFu Building 2, Peking University, 100871 Beijing, People's Republic of China

Open access article: please credit the authors and the full source.

Monitoring and assessing karst rock resulting from desertification is important to local sustainable development in the karst mountain regions of Southwest China. A new derived index, the Normalized Difference Rock Index (NDRI), is proposed to map karst rock. It takes advantage of the unique spectral response of karst rock and other land cover forms. Supervised maximum likelihood classification trials using different input bands (Landsat TM band 3–5, NDVI and NDRI derived from TM imagery) were assessed for accuracy of karst rock mapping in Bijie County, Southwest China. Results were compared with land use maps for 2000, with the best result obtained using a combination of the NDVI and NDRI indices. This paper offers a tool for land cover mapping.

Keywords: Karst rock; desertification; geomorphology; indices; NDRI; mapping; TM image; Southwest China.

Introduction

The karst mountain region of Southwest China is one of the largest karst areas in the world. This karst geomorphology covers about 620,000 km^2, and the ecological environment is extremely fragile (Wang and Liu 2004; Zhang et al 2006). This has led to serious land degradation in the form of desertification: soil is severely or even completely eroded, so that bedrock is exposed over large areas, the carrying capacity of land declines severely, and the landscape resembles a rocky desert because of severe human impacts on the vulnerable eco-geo-environment (La Moreaux et al 1997).

Monitoring and assessing karst rock is important for policy-makers and academic researchers. Traditional methods of mapping karst rock, such as manual interpretation and computer-assisted digital processing of aerial photographs and satellite images, have limitations. Manual interpretation is expensive and laborious and can be used only for a small region. With computer-assisted digital processing, results vary depending on the characteristics of the training samples selected by the analyst, because different analysts do not interpret images in the same manner.

Many techniques have been attempted to map land cover, such as using indices derived from the RS images. A commonly used index is the Normalized Difference Vegetation Index (NDVI), calculated as the difference between the near-infrared and red reflectance values normalized with their sum. For example, Achard and Estréguil (1995) used multitemporal AVHRR mosaics for tropical forest discrimination and mapping, and Fernandez et al (1997) mapped the surfaces affected by large forest fires using NDVI data.

The Normalized Difference Snow Index (NDSI), derived from Landsat Thematic Mapper (TM) bands 2 and 5, (TM2 − TM5) / (TM2 + TM5), has been successfully used to map glaciers in the Illecillewaet Icefield, British Columbia, Canada (Sidjak and Wheate 1999). This index is based on the difference between strong reflection of visible radiation and near total absorption of middle infrared wavelengths by snow (Hall et al 1995a, 1995b). It is effective in distinguishing snow from similarly bright soil, vegetation, and rock, as well as from clouds (Dozier 1989).

The Normalized Difference Water Index (NDWI), calculated as (GREEN − NIR) / (GREEN + NIR), was developed to delineate open water features and enhance their presence in remotely sensed imagery based on reflected near-infrared radiation and visible green light (McFeeters 1996). The selection of wavelengths was done to maximize the typical reflectance of water features by using light wavelengths to minimize the low reflectance of NIR by water features. NDWI may allow turbidity of water bodies to be estimated from remotely sensed data. NDWI is sensitive to changes in the liquid water content of vegetation canopies. It is complementary to but not a substitute for NDVI (Gao 1996).

Few papers focus on methods of mapping barren areas (Jiang et al 2005; Zhao and Chen 2005). Zhao and Chen (2005) used the Normalized Difference Bareness Index (NDBaI, calculated as [TM5 − TM6] / [TM5 + TM6]) to map bare areas. Although the method has good accuracy, it is limited by the use of TM6 (thermal infrared band), which makes it difficult to distinguish barren and built-up areas in the suburban areas where urban heat islands exist.

The objective of the present paper is to offer a new and simple method for mapping karst rock rapidly and accurately. This method is based on the unique spectral response of karst rock and other land cover. The mapping is accomplished through trials using different input bands (Landsat TM band 3–5, NDVI and NDRI derived from TM imagery). The effectiveness of this method was tested by mapping karst rock in Bijie County, Southwest China. Comparison of the results obtained using this method with an existing land use map (2000) demonstrates that it is highly reliable. This method also produces very accurate results more efficiently than supervised classification using only Landsat TM bands.

Study area

Bijie County is in Southwest China (ranging from $104°52'$ to $106°6'$E and from $26°49'$ to $27°46'$N) with an estimated area of 6900 km^2. Karst areas account for 61.9% of the land area (Figure 1; Cai 1990). It is a typical karst rock area with rather severe desertification, the spatial extent of which has drastically expanded during the last decade. The Chinese

Academy of Science submitted two reports to the China central government in 1994 and 2003, proposing comprehensive rehabilitation. Limited by local biophysical conditions and low population density, farmland is scarce and can be ignored. The main land cover areas are needleleaf forest, broadleaf forest, grasslands, and barren karst rock, which account for about 90% of the total surface. Other forms of land cover are a water body and built-up area (mainly the national-level road; Huang and Cai 2007).

Data and methodology

Data sources
A Landsat ETM recorded on 22 May 2001 was acquired from the Global Land Cover Facility at the Institute of Geographic Sciences and Natural Resources Research (http://glcf.geodata. cn). The land use map for the year 2000 at a scale of 1:50,000 was acquired from local Land Management Bureaus.

Methodology
Figure 2 shows the Landsat TM image of the study area on which various surface covers (eg broadleaf forest,
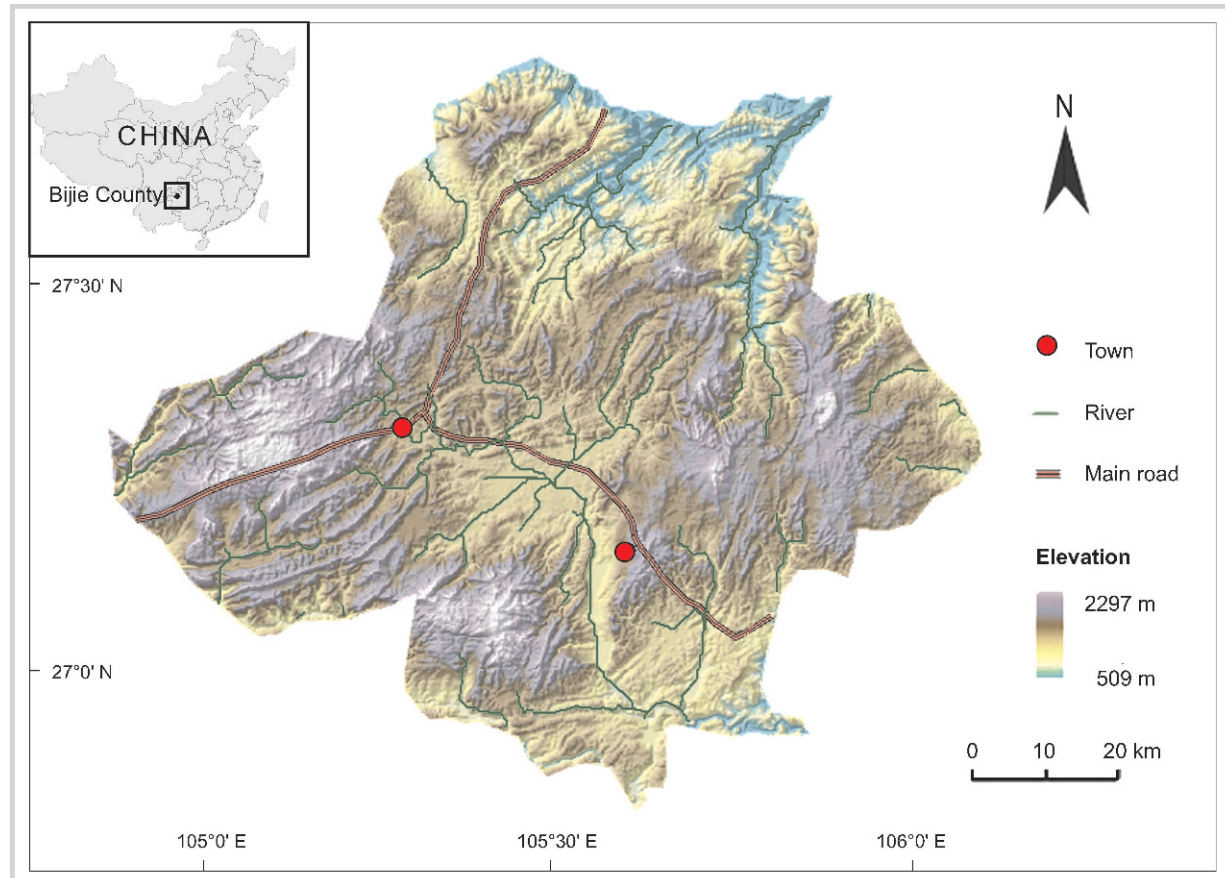
FIGURE 1 Location of study area. (Map by Qiuhao Huang)

FIGURE 2 *Photos on the left:* dispersed (top photo) and continuous (bottom photo) karst rock cover, indicating slight and severe desertification, respectively. *Right:* false color composite of TM bands 4–3–2 (RGB). Major typical land covers shown are needleleaf forest (1), broadleaf forest (2), grassland (3), water (4), built-up areas (5), and karst rock (6 shows dispersed and 7 continuous karst rock). (Photos and map by Qiuhao Huang)
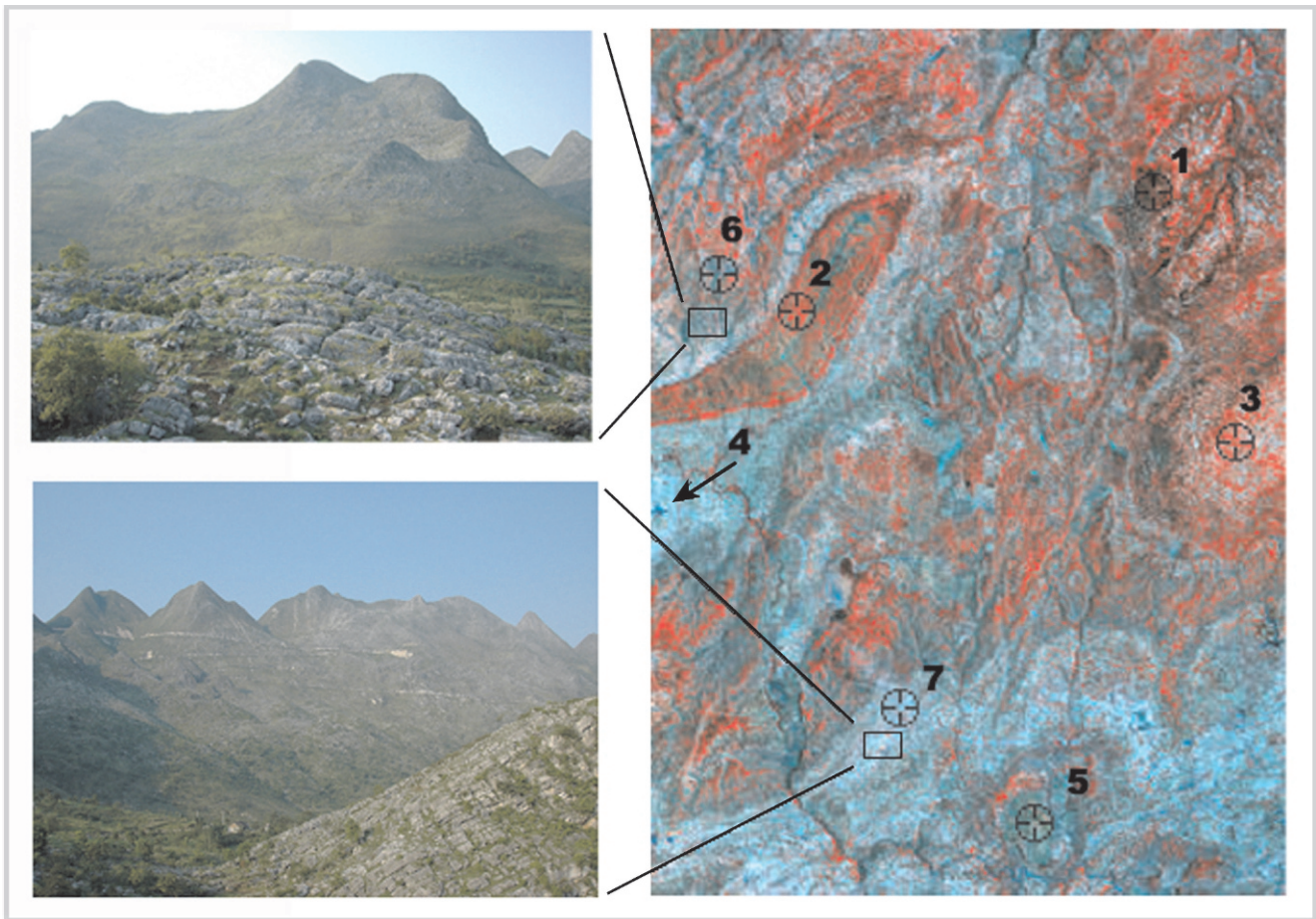
needleleaf forest, grassland, and karst rock) are distinguishable. By repeatedly using the representative pixels of each of these covers (on average 10–15 pixels were groundtruthed), their Digital Number (DN) values in 7 bands were averaged and displayed graphically in Figure 3. This profile illustrates that their spectral disparity is greatest in bands 3, 4, and 5. These values are distinctive from one another. Therefore, they are the most useful bands from which land cover may be potentially differentiated.

A close scrutiny of Figure 3 reveals that except for karst and built-up areas, vegetation (broadleaf forest, needleleaf forest, grassland) has a higher reflectance on band 4. Band 4 exceeds those on band 3. By comparison, all the nonvegetative categories have a smaller pixel value on band 4 than band 3. Therefore, the commonly used index, NDVI (Equation 1), referred to as subtraction of band 3 from band 4, results in positive pixel values for vegetation pixels:

$$NDVI = (band\ 4 - band\ 3)/(band\ 4 + band\ 3). \quad (1)$$

To facilitate subsequent processing, the NDVI image was derived for further analysis.

Vegetation types, karst rock, and built-up areas experience a drastic increase in their reflectance from band 3 to band 5. Water has a slightly smaller pixel value

FIGURE 3 Spectral profiles of the 6 main land cover classes in the study area.
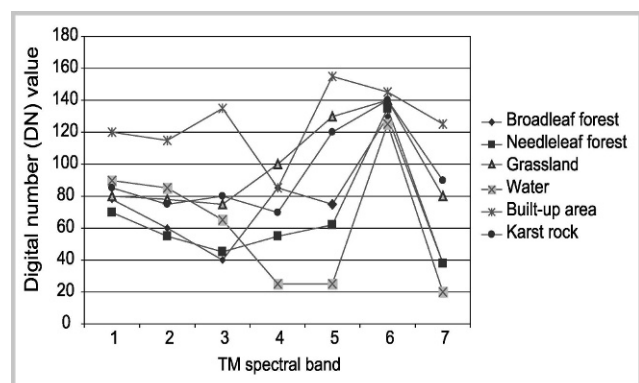
on band 5 than on band 3 (Figure 3). The derived index—the Normalized Difference Rock Index (NDRI)—is a standardized differentiation of these two bands (Equation 2); it was derived using principles similar to those used to derive the NDVI. The NDRI results in negative pixel values for water bodies but positive pixel values for all other land cover classes. The pixel values for water bodies are markedly lower in the fourth and fifth bands, based on the difference between strong reflection of visible radiation and near total absorption of middle infrared wavelengths by water (Hall et al 1995b):

$$NDRI = (band\ 5 - band\ 3)/(band\ 5 + band\ 3). \quad (2)$$

In order to facilitate subsequent processing, the NDVI image was derived for further analysis.

Based on the two indices (NDVI and NDRI), supervised maximum likelihood classification trials were conducted using different combinations of input bands. Preliminary qualitative assessment of classification results was guided by a visual interpretation of the image. Training areas were established for 6 separate classes: needleleaf forest, broadleaf forest, grassland, water, built-up areas, and karst rock. Classification trials were performed with the following band combinations:

1. TM bands 3, 4, and 5
2. NDVI and NDRI
3. TM bands 3–5 and NDRI
4. TM bands 3–5 + NDVI + NDRI.

In the final classification result, dispersed and continuous karst rock (indicating slight and severe desertification) were combined into one category: karst rock.

The classification method of automatic mapping suggested by Zha et al (2003), a binary assessment method, was also used to judge extracting built-up areas and barren lands (such as karst rock) according to the different positive or negative values of each index map. According to this method, the true value of each pixel is recoded to 254 if the NDVI (NDRI) value is positive (+) or to 0 if the NDVI (NDRI) value is negative (−). Table 1 shows that the NDVI and NDRI values for needleleaf forest, broadleaf forest, grassland, and water are all identical (the first three are positive, the last, water, is

negative), but the NDVI and NDRI values for built-up areas and karst rock are quite different. Thus, after subtraction of NDVI from NDRI, the pixels with a value of 254 indicate the area with karst rock. (Because built-up areas in this area are quite limited, they may be counted as karst rock using this method.)

Finally, these classification results were compared with the actual land use map for 2000. Operations to derive NDVI and NDRI, guided maximum likelihood classifications, and recording pixel values were done using the ERDAS software.

Results

Table 2 shows the results of the different land cover classifications using supervised maximum likelihood classification by various band combinations. In this table Trials 1–4 were used to determine maximum likelihood classification by various band combinations. Trial 5 was used with binary judging, and the land cover types were classified into vegetation (including forest and grassland), water, and karst rock (including built-up areas).

Spatial accuracy from spatial pattern was performed in the ArcGIS environment using different band combinations compared with land use in 2000. Several methods exist to assess spatial accuracy in current practice. One is the Kappa statistic (Munroe et al 2002; Pontius 2002); another the Receiver Operating Characteristic (ROC) curve (Pontius and Schneider 2001). In this study we overlaid the different trial maps on the 2000 land use map; then a cell-by-cell comparison of the accuracy of the method was performed to evaluate the predicted versus actual karst rock spatial pattern. This spatial assessment method was also used widely (Pereira and Itami 1991; Bian and West 1997; Narumalani et al 1997). The result is shown in Table 3. Trial 2 shows better performance than other trials for mapping karst rock. The result shows that about 77% of non-karst rock and 82% of karst rock was classified correctly, corresponding to their spatial locations. Figure 4 shows the spatial pattern of actual karst rock using the NDVI and NDRI indices in Bijie County. The results were satisfactory.

TABLE 1 Positive and negative values of each representative land cover class in NDVI and NDRI maps.

Index	Needleleaf forest	Broadleaf forest	Grassland	Water	Built-up area	Karst rock
NDVI	+(254)	+(254)	+(254)	−(0)	−(0)	−(0)
NDRI	+(254)	+(254)	+(254)	−(0)	+(254)	+(254)
NDRI–NDVI	0	0	0	0	254	254

TABLE 2 Results of different land cover classifications.

Classification	Forest (%)	Grassland (%)	Water (%)	Built-up area (%)	Karst rock (%)
Trial 1 (TM 3–5)	28.23	6.53	0.08	6.12	59.04
Trial 2 (NDVI + NDRI)	45.33	7.26	0.07	9.45	37.88
Trial 3 (TM 3–5 + NDRI)	36.55	8.75	0.29	0.75	53.66
Trial 4 (TM 3–5 + NDVI + NDRI)	43.83	0	0.10	0	42.48
Trial 5 (NDRI − NDVI)	62.4	—	1.30	—	36.30
Land use map (2000)	44.63	9.15	0.08	3.13	43.02

TABLE 3 Spatial accuracy of karst rock mapping using different band combinations.

| Trial	Actual land cover classes	Classified land cover classes (km^2)		Accuracy (%)
		Non-karst rock	Karst rock	
1	Non-karst rock	1267	1024	55
	Karst rock	377	1348	58
2	Non-karst rock	1967	581	77
	Karst rock	378	1684	82
3	Non-karst rock	1589	1040	60
	Karst rock	547	1433	72
4	Non-karst rock	1536	1094	58
	Karst rock	490	1490	75
5	Non-karst rock	2002	627	76
	Karst rock	936	1044	53

Discussion

The study area is located in the karst mountain regions of Southwest China, where land degradation is most serious, land surface is uneven, and topographic conditions are complicated. All these factors increase the difficulty of mapping land use precisely. Even the Chinese Academy of Science uses the TM/ETM image to interpret the land use map. The accuracy is merely about 75% before manual adjustment; only after the manual adjustment might the accuracy reach about 85% (Xiong 2002). The new combination of NDVI and NDRI exemplified in this paper can map karst rock at an accuracy level of 80% using supervised classification, and the method is greatly superior to that with TM band supervised classification or the binary judging method. In comparison with combination of TM band supervised classification, the new method enables karst rock areas to be mapped at a higher degree of accuracy. Therefore it could be concluded that the proposed

combination of NDVI and NDRI is much more effective and advantageous in mapping karst rock area than Landsat TM bands when performing maximum likelihood classification. By comparison with the binary judging method, it could distinguish between built-up areas and karst rock. So the method can serve as a worthwhile alternative for quickly mapping karst rock area.

However, it is also important to know the limitations of this method. Sidjak and Wheate (1999) successfully classified iceberg cover with other land cover using NDSI; Zha et al (2003) mapped the built-up area of Nanjing, China, using the NDBI with an accuracy of 94%. In this research, using the derived NDRI, the highest accuracy is only about 80%. Several reasons contribute to incorrect classification of the karst rock, including the following: (1) the pixel values of karst rock and built-up areas are rather close, and it is not easy to differentiate them just through maximum likelihood classification, and (2) Landsat image errors are induced by the sensor system and data

FIGURE 4 Spatial pattern of the classified and actual karst rock cover, using the NDVI and NDRI indices. (Map by Qiuhao Huang)
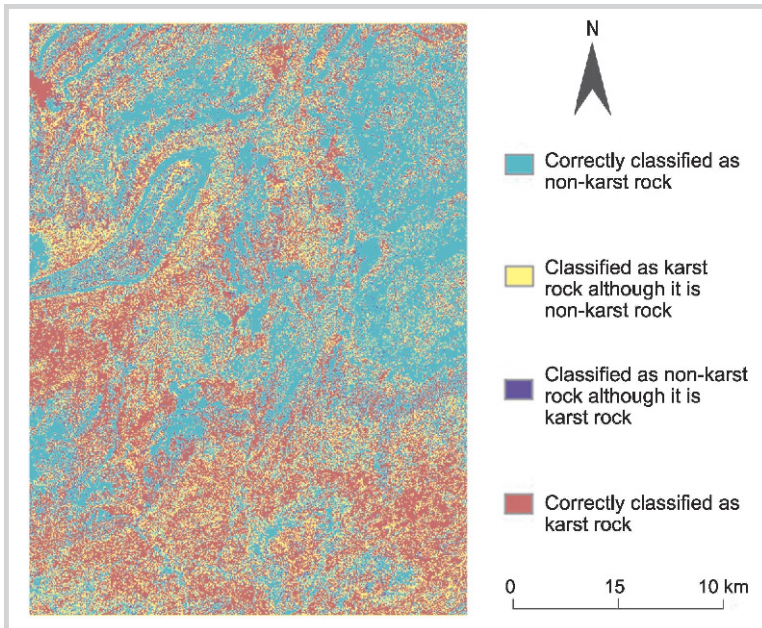
processing, including satellite navigation errors, sensor degradation, data resampling, view and zenith angle change, atmospheric attenuation, and cloud contamination. Especially the former is critical to get an objective result, so it is quite important to select the typical training area carefully for different types of land cover when performing the supervised classification.

Finally, the inherent limitation of NDRI should also be underlined. Given that the NDRI is derived by the same method as the NDVI, it also has the same limitations as NDVI. The most important is seasonality. Because some kinds of land cover—such as grassland and farmland—change considerably depending on the season, it is also possible for the NDRI of one land cover to be positive in summer and negative in winter. Therefore, it is critical to select the appropriate Landsat image for mapping.

Conclusion

This research mapped karst rock using supervised classification of Landsat TM bands 3–5, NDVI, and NDRI. The comparison of the final results shows that the combination of NDVI and NDRI has a greater accuracy than other methods. It appears to be a reasonable method for rapid and efficient estimation of karst rock using digital imagery. The NDRI may also be a useful tool for land cover mapping.

REFERENCES

Achard F, Estréguil C. 1995. Forest classification of Southeast Asia using NOAA AVHRR data. *Remote Sensing of Environment* 54:198–208.
Bian L, West E. 1997. GIS modeling of elk calving habitat in a prairie environment with statistics. *Photogrammetric Engineering and Remote Sensing* 63:161–167.
Cai YL. 1990. *The Territorial Structure and Resources Development in Guizhou Province, China* [in Chinese with English abstract]. Beijing, China: China Ocean Press.
Dozier J. 1989. Spectral signature of Alpine snow cover from the Landsat Thematic Mapper. *Remote Sensing of Environment* 28:9–22.
Fernandez A, Illera P, Casanova JL. 1997. Automatic mapping of surfaces affected by forest fires in Spain using AVHRR NDVI composite image data. *Remote Sensing of Environment* 60:153–162.
Gao BC. 1996. NDWI: A normalized difference water index for remote sensing of vegetation liquid water from space. *Remote Sensing of Environment* 58:257–266.
Hall DK, Foster JL, Chein JYL, Riggs GA. 1995a. Determination of actual snow covered area using Landsat TM and digital elevation model data in Glacier National Park, Montana. *Polar Record* 31:191–198.
Hall DK, Riggs GA, Salomonson VV. 1995b. Development of methods for mapping global snow cover using Moderate Resolution Imaging Spectroradiometer data. *Remote Sensing of Environment* 54:127–140.
Huang Q, Cai Y. 2007. Spatial pattern of karst rock desertification in the middle of Guizhou Province, southwestern China. *Environmental Geology* 52(7):1325–1330.
Jiang J, Zhou J, Wu H, Ai L, Zhang H, Zhang L, Xu J. 2005. Land use/cover changes in the rural–urban interaction of Xi'an region, West China, using Landsat TM/ETM data. *Agrifood Research Reports* 68:328–340.

La Moreaux PE, Powell WJ, Le Grand HE. 1997. Environmental and legal aspects of karst areas. *Environmental Geology* 29:23–36.
McFeeters SK. 1996. The use of the Normalized Difference Water Index (NDWI) in the delineation of open water features. *International Journal of Remote Sensing* 17:1425–1432.
Munroe DK, Southworth J, Tucker CM. 2002. The dynamics of land-cover change in western Honduras: Exploring spatial and temporal complexity. *Agricultural Economics* 27:355–369.
Narumalani S, Jensen JR, Althausen JD, Burkhalter S, Mackey HE Jr. 1997. Aquatic macrophyte modelling using GIS and multiple logistic regression. *Photogrammetric Engineering and Remote Sensing* 63:41–49.
Pereira JMC, Itami RM. 1991. GIS-based habitat modeling using logistic multiple regression: A study of the Mountain Graham red squirrel. *Photogrammetric Engineering and Remote Sensing* 57:1475–1486.
Pontius RG Jr. 2002. Statistical methods to partition effects of quantity and location during comparison of categorical maps at multiple resolutions. *Photogrammetric Engineering and Remote Sensing* 68(10): 104–1049.
Pontius RG Jr, Schneider LC. 2001. Land-cover change model validation by an ROC method for the Ipswich watershed, Massachusetts, USA. *Agriculture, Ecosystems and Environment* 85:239–248.
Sidjak RW, Wheate RD. 1999. Glacier mapping of the Illecillewaet icefeld, British Columbia, Canada, using Landsat TM and digital elevation data. *International Journal of Remote Sensing* 20:273–284.
Wang S, Liu Q. 2004. Karst rocky desertification in southwestern China: Geomorphology, land use, impact and rehabilitation. *Land Degradation and Development* 15:115–121.

Xiong K. 2002. *The Study of Karst Rocky Desertification Using the GIS and RS Tech: A Case Study of Guizhou Province, China* [in Chinese with English abstract]. Beijing, China: China Geology Press.

Zha Y, Gao J, Ni S. 2003. Use of normalized difference built-up index in automatically mapping urban areas from TM imagery. *International Journal of Remote Sensing* 24:583–594.

Zhang B, Xiao F, Wu H, Mo S. 2006. Combating the fragile karst environment in Guizhou, China. *Ambio* 35:94–96.

Zhao H, Chen X. 2005. Use of Normalized Difference Bareness Index in quickly mapping bare areas from TM/ETM+. *IEEE International Geoscience and Remote Sensing Symposium (IGARSS)* 3:1666–1668.